ADVANCED MATERIALS INTERFACES
Open Access
www.advmatinterfaces.de

Hydrogel-Based Flexible Energy Storage Using Electrodes Based on Polypyrrole and Carbon Threads

Jean G. A. Ruthes, Andrei E. Deller, Emmanuel Pameté, Izabel C. Riegel-Vidotti, Volker Presser, and Marcio Vidotti**

Developing new flexible and electroactive materials is a significant challenge to producing safe, reliable, and environmentally friendly energy storage devices. This study introduces a promising electrolyte system that fulfills these requirements. First, polypyrrole (PPy) nanotubes are electropolymerized in graphite-thread electrodes using methyl orange (MO) templates in an acidic medium. The modification increases the conductivity and does not compromise the flexibility of the electrodes. Next, flexible supercapacitors are built using hydrogel prepared from poly(vinyl alcohol) (PVA)/sodium alginate (SA) obtained by freeze–thawing and swollen with ionic solutions as an electrolyte. The material exhibits a homogenous and porous hydrogel matrix allowing a high conductivity of 3.6 mS cm^{-1} as-prepared while displaying great versatility, changing its electrochemical and mechanical properties depending on the swollen electrolyte. Therefore, it allows its combination with modified graphite-thread electrodes into a quasi-solid electrochemical energy storage device, achieving a specific capacitance (C_s) value of 66 F g^{-1} at 0.5 A g^{-1}. Finally, the flexible device exhibits specific energy and power values of 19.9 W kg^{-1} and 3.0 Wh kg^{-1}, relying on the liquid phase in the hydrogel matrix produced from biodegradable polymers. This study shows an environment friendly, flexible, and tunable quasi-solid electrolyte, depending on a simple swell experiment to shape its properties according to its application.

1. Introduction

Flexible and wearable electronics have gained increasing significance across diverse technology sectors, including healthcare, automotive, aerospace, and energy systems. However, developing energy storage devices capable of powering these electronics is challenging, as the performance of these devices heavily depends on the properties of electrode materials and electrolytes. Researchers have been dedicating considerable attention to developing high-performance flexible electrodes and electrolyte materials to enhance these devices' energy and power densities.[1] Carbon-based materials, including fibers, rods, cloth, and powder, have been extensively investigated as potential electrodes for electrochemical energy storage. This is due to their high electrical conductivity, chemical stability, exceptional malleability, and large surface area.[2] These materials can be modified using electrochemical or chemical methods, allowing the combination of their inherent properties with different compounds such as transition metal oxides and polymers, as well as their unique structures such as 2D graphene and 3D nanotubes, making them highly versatile for use in various electrochemical technologies.[3] Flexible energy storage devices are an area of active research involving these materials, as their qualities can be further improved through straightforward modifications, making them suitable for use in different electrochemical energy storage technologies.[4]

J. G. A. Ruthes, A. E. Deller, I. C. Riegel-Vidotti, M. Vidotti
Grupo de Pesquisa em Macromoléculas e Interfaces, Departamento de Química
Universidade Federal do Paraná (UFPR)
Curitiba 81531-98 0, Brazil
E-mail: mvidotti@ufpr.br

J. G. A. Ruthes, E. Pameté, V. Presser
INM – Leibniz Institute for New Materials
D2 2, 66123 Saarbrücken, Germany
E-mail: volker.presser@leibniz-inm.de

J. G. A. Ruthes, V. Presser
Department of Materials Science and Engineering
Saarland University
Campus D2 2, 66123 Saarbrücken, Germany

V. Presser
saarene – Saarland Center for Energy Materials and Sustainability
Campus C4 2, 66123 Saarbrücken, Germany

The ORCID identification number(s) for the author(s) of this article can be found under https://doi.org/10.1002/admi.202300373

DOI: 10.1002/admi.202300373

One useful approach for enhancing the performance of flexible energy storage devices is to modify electrode materials, focusing on the final application in terms of energy delivery. Supercapacitors offer a faster charge–discharge rate and long cycle life than batteries. This relates to the rapid charge transfer of electrosorption (electrical double-layer capacitors) or pseudocapacitive redox processes (pseudocapacitors) at the expense of affording a lower energy density.[5] The spectrum of reported supercapacitor electrodes is broad and includes nanoporous carbons, pseudocapacitive materials (such as layered metal oxides and MXene), and redox-active polymers.[6] Among the materials used for carbon modifications, aromatic conductive polymers have been widely used for electrochemical energy storage due to their excellent physicochemical properties, such as high conductivity and chemical and mechanical stability.[7] Amid these polymers, polypyrrole (PPy) has emerged as a promising candidate for electrochemical energy storage due to its high conductivity and electroactivity. However, its practical application is limited by poor stability during charge–discharge cycling, attributed to the mechanical stress of the polymeric structure during operation.[8] Therefore, researchers have focused on developing novel approaches to enhance the stability and performance of PPy electrode materials for flexible electrode development.

Along with a good electrode material, the choice of electrolyte is critical in developing high-performance flexible energy storage devices. A suitable electrolyte must possess key properties such as a large potential stability window, high conductivity, low viscosity, high electrochemical stability, nonflammability, and environmental friendliness.[9] While aqueous, organic, or ionic liquids are commonly used, they pose risks such as toxicity, corrosiveness, and low potential.[10] Hydrogels have been explored as an electrolyte media for quasi-solid-state and solid-state devices to overcome these limitations. Polyvinyl alcohol (PVA) is a promising compound precursor for hydrogel synthesis due to its chemical stability, nontoxicity, elevated viscosity, and biodegradability.[11] The properties of PVA-based hydrogels can be attributed to the line polymer chains with hydroxyl groups that allow for hydrogen bonding with water molecules, leading to significant swelling of aqueous solutions into the chemical structure of the hydrogel, resulting in modifications to properties such as ionic conductivity and mechanical resistance.[12] Additionally, the combination of polymer extract from brown algae, sodium alginate (SA) in the synthesis enhances mechanical properties due to the formation of cross-linking chains in the gel matrix, orientated by the hydroxyl-carboxyl groups interactions of the polymers.[13] These interactions allow easy modification of both ionic conductivity and mechanical aspects of the hydrogel by swelling, reducing the risks of liquid electrolytes while maintaining high water content and similar conductivity.[14] Additionally, these hydrogels also display attractive properties for wearable applications such as stretchability, self-healing and biocompatibility.[13a,15]

In this work, we present a flexible electrochemical energy storage device that utilizes modified graphite electrodes and a PVA/SA hydrogel electrolyte. The graphite threads were functionalized with PPy nanostructures through electropolymerization, resulting in electrodes with increased electrical conductivity and specific capacitance (C_s) while retaining flexibility. These electrodes were then incorporated into a PVA/SA hydrogel electrolyte, prepared using a simple freeze–thaw method, which exhibited high conductivity and tunable properties through swelling experiments. This combination enabled the facile and versatile assembly of a flexible energy storage device that displayed pseudocapacitive behavior.

2. Results and Discussion

3. Electrode Characterization

The electrodes feature thin graphite threads, as shown in the scanning electron micrographs in **Figure 1**. The pristine graphite threads are about 5 µm in diameter, with high compaction and uniform morphology, observed in Figure 1A. The electropolymerization yields a PPy nanoparticle decoration of the graphite wires, as seen in Figure 1B and Figure S1C,D (Supporting Information). Agglomerates of interconnected structures such as cylinders indicate the deposition of PPy nanotubes, which aim to increase the surface area and allow more charge transfer, enhancing the conductivity of the electrode.[19] Transmission electron microscopy (TEM) analysis (Figure 1C,D) confirmed the presence of nanostructures morphology and geometry of the substrate. The deposition of nanotubes occurred parallel to the surface of the wire, as evidenced by the protuberant structures shown in Figure 1C,D, along with nanoparticles over the measured surface.[20] Figure S1A (Supporting Information) displays the pristine electrodes, showing that each graphite thread of the yarn acts as an electrode. Microscopy analysis suggests that the interconnected structures were distributed over the surface of each thread, which could enhance the conductivity and structure of the electrode, as shown in Figure S1B–F (Supporting Information) displays. Although the geometry of the yarn is not ideal, the representative images exhibit the characteristic structure of PPy nanotubes polymerized over different substrates such as carbonaceous, stainless steel, composites, and others.[20,21] Further investigation of the polymer modification was carried out using spectroscopy techniques.

Fourier transform infrared (FTIR) and Raman were used to evaluate the structural characterization of the modification. **Figure 2**A displays the FTIR spectrum of the electrodes where is exhibited the characteristic PPy bands: 1543 cm^{-1} C=C stretching, 780, and 669 cm^{-1} related to C−H out-of-ring plane deformation of the pyrrole (Py) ring. Also, we see the influence of methyl orange (MO) used as a framework molecule. The Raman spectrum in Figure 2B displays characteristic bands of PPy nanotubes 986 cm^{-1} ring deformation, 1051 cm^{-1} in plane C−H bending, 1324 cm^{-1} PPy ring stretching, and 1598 cm^{-1} related to the C=C vibration.[22] In addition, the influence of MO is visible with distinctive bands at 1116 cm^{-1} SO− stretching and 1365 cm^{-1} S-ring and C−C stretch, indicating the presence of the framework, which could act on doping the polymer.[23]

The modified electrode was further examined by X-ray diffraction (XRD), the diffractograms shown in Figure 2C, after subtracting a straight baseline and approximating the background contribution, as reported by Ricciardi et al.[12c] The diffractograms indicate the presence of the characteristic broad peak centered close to 25°, which is associated with the π–π interaction of the polymer chains, suggesting the orientation of the chemical structure.[20,21] The average dimensions for the PPy nanotubes are presented in Figure 2D.

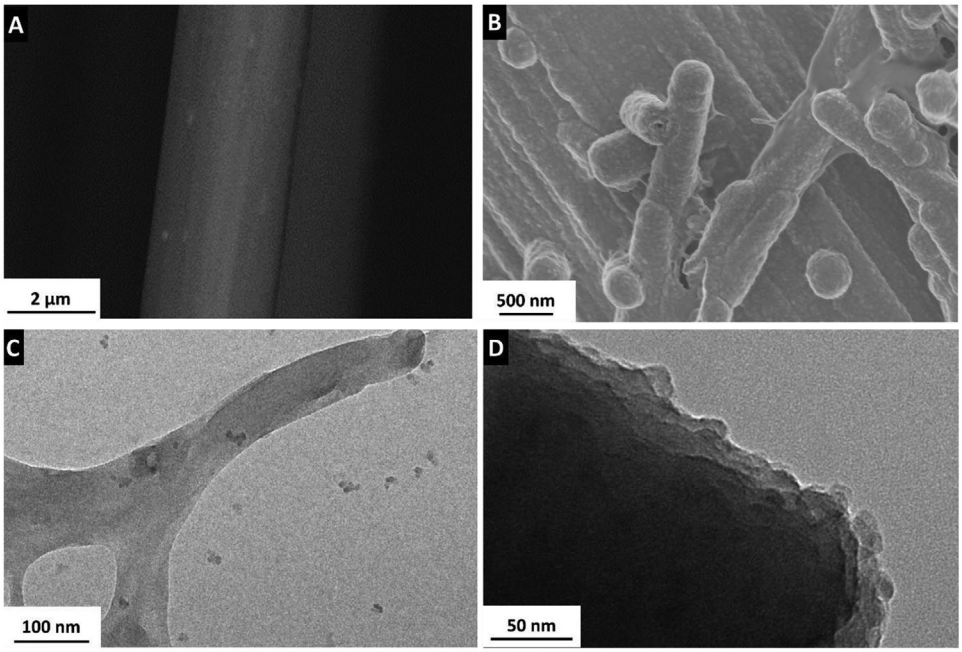

Figure 1. Morphologic characterization of the electrodes. Representative scanning electron micrographs of the electrodes. A,B) Graphite threads modified with polypyrrole (PPy) nanotubes. C,D) Transmission electron micrographs of modified graphite threads with PPy nanotube electrodes.

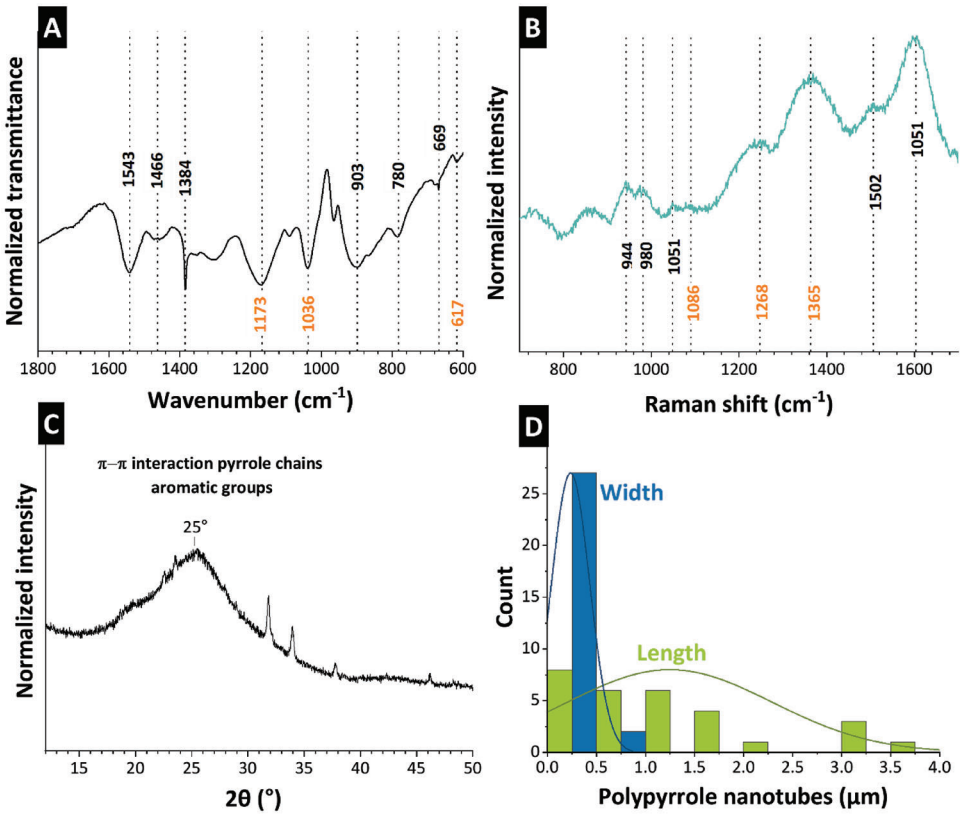

Figure 2. Structural characterization of the polymeric structures. A) FTIR spectra and B) Raman spectra were recorded with a 633 nm laser excitation line. C) X-ray diffractograms of modified graphite threads with PPy nanostructures in the presence of MO. D) Average dimensions of PPy nanotubes.

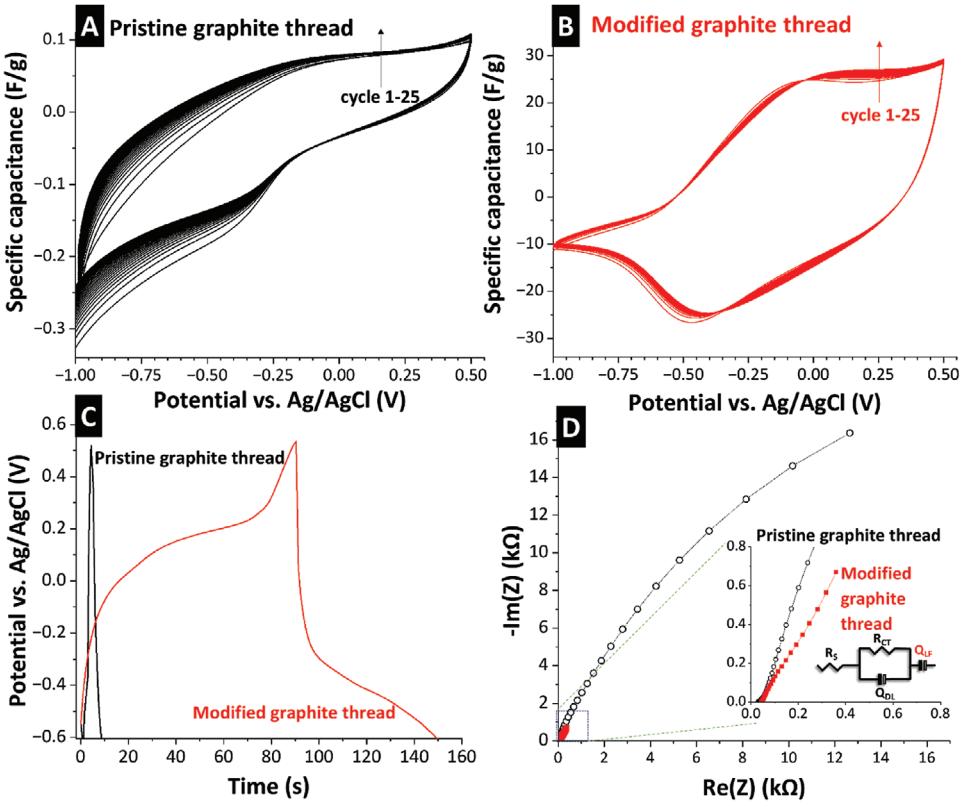

Figure 3. A) Cyclic voltammograms recorded at 100 mV s^{-1} in 0.5 M Na_2SO_4 of pristine graphite electrodes. B) Cyclic voltammograms recorded at 100 mV s^{-1} in 0.5 M Na_2SO_4 using modified graphite electrodes with PPy nanotubes. C) Galvanostatic charge potentially limited the electrodes and D) Nyquist impedance spectra of graphite threads pristine and modified with PPy nanotubes.

The electrochemical properties of the polymerization were investigated. Cyclic voltammograms of the 25 cycles of pristine graphite thread modified with PPy are shown in **Figure 3**A,B. The modified electrode displayed a distortion in the shape of the curve and an increased specific C_s, both associated with the polymer faradaic behavior, which facilitates ionic diffusion during the charge transfer. This can be explained by the polymer 3D interconnected structure, which enables the counterions to access more internal redox-active sites, favored by the charge delocalization on the polymer chains.[21c,23a] Moreover, GCPL curves presented in Figure 3C display a similar distortion of the triangular shape from the pristine thread to a Faradaic due to polymerization, indicating the effect of the doping molecule (MO) on the conductivity.[20,24]

The impedance spectra were analyzed according to the equivalent circuit, both displayed in Figure 3D. The circuit is set by a serial resistance (R_s) associated with the resistance of the solution, intrinsic resistance of the electrode, and connection resistance to the measuring equipment. In series to R_s is a charge-transfer resistance (R_{ct}) element that is related to a charge-transfer process, followed by a constant phase element (C_{DL}) correlated to the electric double-layer C_s.[25] In the modified electrode equivalent circuit, we applied a constant phase element (C_{LF}) related to the low-frequency C_s to account for charge intercalation.[23a,26] The calculated parameters are shown in **Table 1**.

The difference in R_s can be attributed to the intrinsic resistance of the material related to the electrode, considering that electrolyte, electrical connections, and distance between electrodes were the same for all analyses. The modification with PPy nanotubes lowered the value of R_s, favoring electronic transfer onto the electrode. Additionally, the decrease of R_{ct} value after the modification indicates facilitation of charge transfer, therefore benefitting Faradaic reactions,[27] as can be seen in the voltammogram in Figure 3A as a high increase of the current intensity, and in Figure 3B as a shift in the redox potentials.

Table 1. Calculated parameters of equivalent circuit components.

Sample	R_s [Ω]	R_{ct} [Ω]	C_{DL} [F s^{n-1} g^{-1}]	n_{DL}	C_{LF} [F s^{n-1} g^{-1}]	n_{LF}
PG	36.1	43882.0	0.000379	0.796	–	–
G@nPPy	15.1	41.6	0.000739	0.599	0.01045	0.612

PG: Pristine graphite thread; G@nPPy: graphite threads modified with PPy nanostructures.

The constant phase element in the high-frequency C_{DL} is related to the electric double-layer C_s of the electrodes, which is associated with changes in the morphology with the electrodeposition of PPy nanotubes structures shown in scanning electron micrograph (Figure 1). Therefore, the nanotubes increased the surface area of the electrode and allowed the adsorption of ions in the double layer, increasing its value. As for the low-frequency region of the Nyquist plot, a constant phase element C_{LF} is applied to the modified electrode and is related to the charge intercalation process inside the 3D interconnected nanotubes,

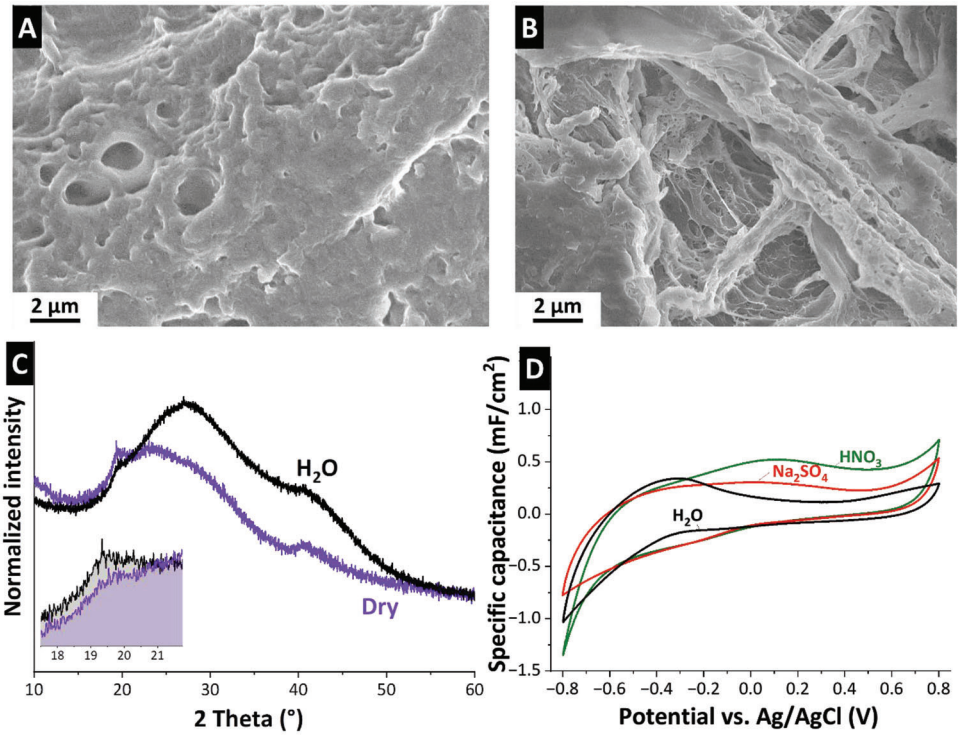

Figure 4. A,B) Representative scanning electron micrographs of as-prepared and freeze-dried hydrogel, respectively. C) X-ray diffractograms of hydrogel samples dry and swollen with H_2O. D) Swelling experiments of dry and wet hydrogel samples with solutions HNO_3, Na_2SO_4, and distilled water. D) Cyclic voltammograms at 50 mV s^{-1} with hydrogel samples swollen in three different solutions.

therefore, indicating a facilitation counter ion intercalation on the redox process by allowing more electroactive sites of the polymer on reaction.[8c] The factors n_{DL} and n_{LF} are associated with the flatness (homogeneity) of the electrode's surface, where one means a perfectly flat surface. The charge intercalation does not occur on the surface of the pure graphite electrode once its surface is very homogeneous and flat, as shown in the scanning electron micrographs. Accordingly, the higher value of n_{DL} when compared with the modified electrode.

The modified electrode holds a smaller value of n_{DL} and an $n_{Lf\,far}$ from one, indicating a very rough surface due to the deposition of the nanotubes. This aligns with the morphological observations from the scanning electron micrographs shown in Figure 1B–D. Electropolymerization of PPy creates nanotubes and, thereby, increases the electroactive surface area of the electrode. This increased specific C_s, exhibiting Faradaic behavior due to the active participation of the polymer in charge-transfer reactions, thereby enhancing its conductivity.

4. PVA-SA Hydrogel Characterization

The quasi-solid pristine hydrogel was stable and conductive in room temperature, maintaining its stability and flexibility even while swelled with different solutions in sequence, as shown in Figure S2 (Supporting Information). Scanning electron microscopy (SEM) images of the cross-section morphology of hydrogel structures: as-prepared and freeze-dried, are presented in **Figure 4**A,B, respectively. As displayed, the as-prepared sample (Figure 4A) indicates a homogeneous material with amorphous and rough morphology, with pores associated with SA presence. The freeze-dried (Figure 4B) sample presented a different morphology, nonporous, and with fibrous-like structures due to the polymeric network's shrinkage during the freeze–thawing and drying cycles, suggesting high crosslink of PVA chains.[14b,16a] Higher magnification images are presented in Figure S3A,B (Supporting Information) of as-prepared, displaying agglomerate structures of PVA formed during freeze–thaw cycles, also presenting the dimensions of the pores.[28] Different cross-section images of the dried sample are shown in Figure S3C–F (Supporting Information), highlighting the material's high porosity, along with the previously mentioned shrinkage of the polymeric chains.

X-ray diffractograms of dry and wet samples are presented in Figure 4C. The dry samples display the distinct PVA peak at 21° (2θ) associated with its reflection planes (101) and ($10\bar{1}$), the semicrystalline nature of SA was observed by the broad peak at 41° 2θ .[12c,29] However, the sample swollen with distilled H_2O diffractogram indicates broadening and shift of the peaks from both polymers, suggesting a loss in crystallinity due to interaction between the polymeric chains and the water molecules. This also shows cross-link behavior in the hydrogel matrix, as hydrogen bonding occurs between the hydroxyl groups of PVA and carboxyl and hydroxyl groups of SA.[12c,30]

To better understand the electrochemical behavior of the hydrogel, the samples dry and wet (with distilled water from synthesis inside the matrix) were immersed in solutions of distilled water, 0.1 M HNO_3, and 0.5 M Na_2SO_4 for 1 h for swelling, controlling the mass variation, and the curves of swelling are present

in Figure S4A,B (Supporting Information). In the dry sample, the electrolytic solution uptake is optimal, easily inserting ionic solutions by a simple soaking process. However, the wet sample indicated a different behavior when soaked into a Na_2SO_4 solution. Due to the significant difference in the concentration of sodium ions between the solution and hydrogel, the liquid phase was expelled from the porous matrix. This process resulted in a more compact and rigid material, as indicated by stiffness analysis in Figure S4E,F (Supporting Information).[12d]

After the thawing process, we also determined the conductivity of the synthesized PVA:SA hydrogel, swollen with pure water and at room temperature. Using electrochemical impedance spectroscopy (EIS) in a two-electrode configuration, the hydrogel was pressed between two stainless steel mesh (with delimited areas ($A = 0.785$ cm^2) and separated by 1 cm (thickness of the hydrogel). The Nyquist plot presented in Figure S4C (Supporting Information), shows the EIS data of the pure hydrogel measured in different periods to evaluate the influence of liquid phase evaporation on the ionic conductivity. The data indicate a very porous gelatinous matrix of the hydrogel affected by the diffusion inside the polymeric structure of the hydrogel, visualized within the lower frequency region. The model circuit of the system shown in the spectrum presents a solution resistance component (R_s) in series with a Warburg element (W_o) related to the influence of the mass transport of electroactive species inside the gel matrix and a constant phase element (C_{DL}) in parallel related to the formation of the electric double layer.[17a]

The obtained R_s value was 359.0 ± 1.3 Ω cm^{-2} in the high frequencies, denoted by the imaginary and real axis intersection. From Equation (1), the ionic conductivity obtained in the hydrogel was 3.6 ± 0.0 mS cm^{-1}, higher than the 3 mS cm^{-1} reported by Jiang et al.[31] This value is superior and comparable to other types of hydrogels previously reported, such as PVA/potassium borate/KCl/H_2O 1.0 mS cm^{-1},[32] CS-TF-10%$LiBF_4$ 2.7 mS cm^{-1},[17a] H_3PO_4/PVA (1:1.5) 3.4 mS cm^{-1},[33] and PAA-PAH (1 M LiCl) 50 mS cm^{-1}.[34]

To further explore the electrochemical stability of the hydrogel, the material was analyzed with two different electrolyte solutions (acidic 0.1 M HNO_3, pH 2.4, and neutral 0.5 M Na_2SO_4 pH 7.1). After the swelling process, the samples were submitted to cyclic voltammetry (CV) in a three-electrode electrode system using two stainless steel meshes as working and counter electrodes and an Ag/AgCl as a reference. The introduction of ionic solutions increased the conductivity of the hydrogel, as shown in Figure 4D. Furthermore, using electroactive solutions to introduce charge carriers in the matrix of hydrogels shapes its properties, making it more conductive and flexible.[31,35] Along with the change in specific current, the peaks shift, suggesting the charge carriers from the electrolytic solutions adsorb at the interface with the electrode. The peak associated with the oxidation of PVA is less intense and shifted to 0.2 V, indicating a diminishment in the oxidation of the polymer.[35a] Furthermore, the interaction between charge carriers and the eggshell polymer chain of the alginate is favored, indicated by the increase of intensity on the peak at −350 mV, suggesting that ionic media directly interacts with the carboxylic groups of the polymer chains.[35b,36] Also, the voltammogram indicates a shift toward behavior slightly pseudocapacitive, as seen from an increase of charges in the system and the more distinctive redox peaks, reinforcing the indication of a stable electrochemical material. Moreover, the increment in the current density is associated with the ionic mobility inside the gel. In contrast, the acidic media was more conductive due to the smaller ionic radius with higher mobility.[11,15c]

The voltammograms are presented in Figure S4D (Supporting Information) of the hydrogel pure after thawing presented to be very stable when evaluated in different scan rates ranging from 10 to 100 mV s^{-1}, with no indication of an irreversible redox process. The specific current increases along with the scan rate range, suggesting a shift in the oxidation peak potential at −500 mV versus Ag/AgCl, related to the reversible redox process with PVA macromolecules at the interface with the electrode.[35a] Also, the small alginate reduction peak at −150 mV versus Ag/AgCl, is caused by the interaction of the carboxylic groups of the eggshell polymeric structure with ions during polarization, which directly affects the diffusion behavior while maintaining chemical stability.[35b,36,37]

Furthermore, the electrolyte material also displayed to interesting highlights such as the ability to recover its conductivity after being fully dried and swelled, and self-healing ability, displayed in Figures S5 and S6 (Supporting Information), respectively.

5. Quasi-Solid-State Assembly and Electrochemical Characterization

With the results of the characterization of the electrodes and hydrogel, a device was assembled with two sets of strings of graphite wires modified with PPy nanotubes introduced parallelly into the hydrogel and sealed into a pouch cell. The potential window of 0 V to +0.6 V was surveyed at 2 mV s^{-1} with 0.5 M Na_2SO_4 as electrolyte swollen into the hydrogel matrix. Also, the device was electrochemically characterized while submitted to constant mechanical stress, bent at a 90° angle during experiments and after to evaluate the properties recovery. The selection of a neutral electrolyte was motivated by the objective of enhancing environmental sustainability for the final device. Nevertheless, an additional investigation was conducted using an acidic electrolytic media of 0.1 M HNO_3 to assess the impact over the device performance. The corresponding data can be found in Figure S7 (Supporting Information) of this work. Moreover, photographs of the electrode and electrolyte are presented in Figure S8 (Supporting Information) illustrating the interface between the materials.

The cyclic voltammograms in **Figure 5**A indicate that the device presented a capacitive behavior with a quasi-rectangular shape as the potential window increased to 0.6 V, with no irreversible redox reaction. This behavior can be associated with the liquid phase, which allows more charge carriers to interact on the surface of the electrodes, suggesting that the electrolyte balances the charge neutrality in the matrix hydrating counteranions.[14a] The electrochemical results of the device, as shown in Figure 5B, when bent at a 90° angle, revealed a significant decrease in C_s and a distorted quasi-rectangular voltammogram, suggesting the occurrence of redox reactions. Upon restoration to its original configuration, the overall shape of the cyclic voltammogram was retained. However, the specific C_s further decreased, indicating degradation or loss of the polymer during the charge–discharge cycles.

The Nyquist plots presented in Figure 5C indicate ion diffusion kinetic, observed by the inclination on the low-frequency

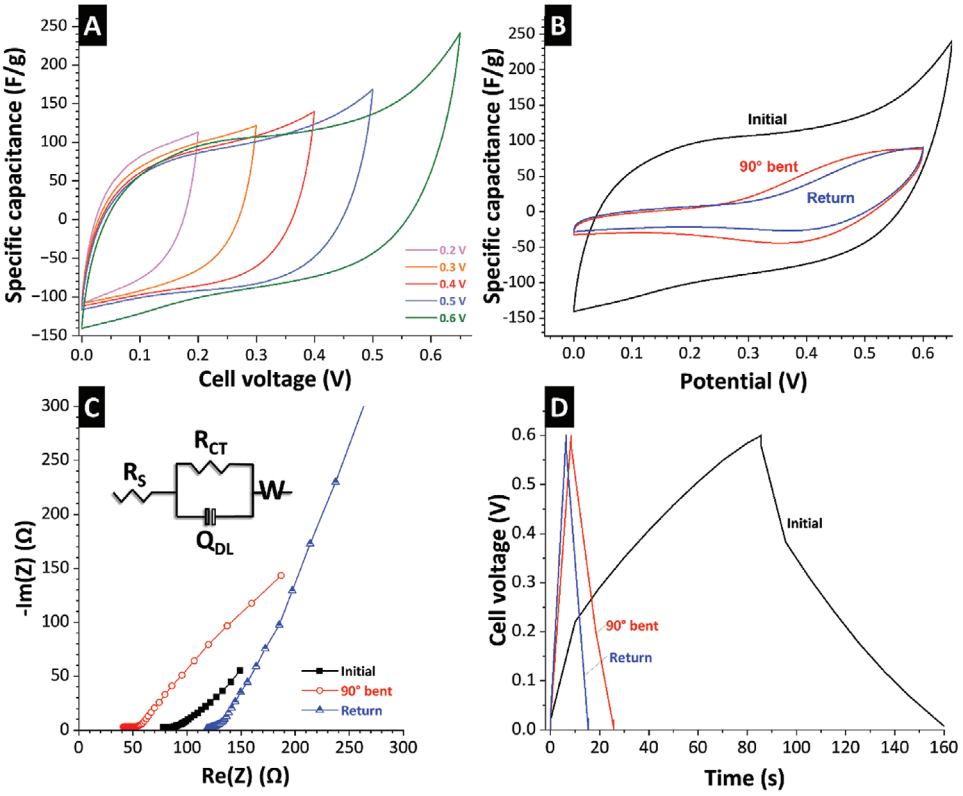

Figure 5. Cyclic voltammograms at 2 mV s^{-1} with A) different maximum cell voltage and B) with different mechanical conditions. C) Nyquist plots of the device in different mechanical stress conditions. Inset: enlargement of the high-frequency region of the plots. D) Galvanostatic charge potentially limits the device in different mechanical stress conditions.

range, elucidating that the conductivity of the hydrogel is related to the aqueous electrolyte swollen into the solid phase.[38] The spectra also suggest a change in the kinetic behavior of the system when inflected with a constant load, which was investigated using the equivalent circuit displayed within the spectra. The calculated parameters are shown in **Table 2**. R_{ESR} is the intrinsic resistance associated with the electrode and the quasi-solid electrolyte. Bending the device to a 90° angle reduces the R_{ESR} value due to a compression of the solid phase. The mechanical stress enables a better interface of the liquid phase with the electrodes. Once the mechanical load is removed, the R_{ESR} increases to a value higher than initially, suggesting a negative impact on both the electrode-electrolyte interface and conductivity of the system as the ions of the liquid phase are no longer evenly distributed in the solid phase of the hydrogel. This aligns with a reduction of the R_{CT} values, indicating that more charge transfer processes occur at the electrode surface.[39] The decreased values of such parameters show the effect of the mechanical load on the displacement of the liquid phase, which allows the charge carriers to reach more intern regions of the nanostructures of PPy .

Parallel to the R_{CT}, a constant phase element (Q_{DL}) is associated with forming an electrical double-layer, representing the charges adsorbed on the electrode surface and located at the interface between the electrode and electrolyte. Along with the element, the factor n_{DL} represents the interface's homogeneity, where values near 1 suggest a homogenous and planar interface between electrode and electrolyte. During mechanical stress, Q_{DL} analysis indicates that fewer charges compose the EDL. However more organized as the n_{DL} values increase. Upon removal of mechanical stress, the charge carriers are occluded on the 3D structure of PPy nanotubes and more distributed, increasing the value of Q_{DL}, corroborating with the increase in the diffusion resistance, indicated by the rise in W values. This observation was previously observed in PPy films and nanostructures electrochemical systems interpreted as equilibrium insertion C_s.[24,40]

Table 2. Calculated parameters of equivalent circuit components for the device swollen with 0.5 M Na_2SO_4.

Sample	R_s [Ω]	R_{ct} [Ω]	C_{DL} [F s^{n-1}]	n_{DL}	Z_W [Ω]	Q_{Lf} [F s^{n-1}]	n_{LF}	k_1	k_2
Initial	57.78	54.26	6.73×10^{-3}	0.119	51.7	9.38×10^{-3}	0.513	0.37	0.48
90°-bent	28.30	33.55	1.56×10^{-3}	0.255	139.5	1.68×10^{-3}	0.835	0.05	0.23
Return	62.88	73.20	2.135×10^{-4}	0.583	140.3	1.26×10^{-4}	0.735	0.001	0.02

Table 3. Literature reports on other hydrogel energy storage devices compared to the present work.

Hydrogel	Liquid phase electrolyte	Electrode	Specific capacitance (C_s)	Reference
PVA: Alg Freeze–thawed (10:1)	0.5 M Na_2SO_4 (swollen)	Graphite threads modified with PPy nanotubes	66 F g^{-1} @ 0.5 A g^{-1}	Present work
PVA-TA	2.8 M H_3PO_4 (swollen)	PANI@CNT	58 F g^{-1} @ 0.3 A g^{-1}	[47]
PVA-potassium Borate	30×10^{-3} M KCl (in situ)	AC	38 F g^{-1} @ 0.5 A g^{-1}	[47]
PVA/Gly	2.4 M CH_3COONa (in situ)	AC	26 F g^{-1} @ 0.3 A g^{-1}	[47]
PVA-MBAA	$EMimBF_4$	rGO	31 F g^{-1} @ 0.1 A g^{-1}	[48]
Alg/$EMImBF_4$	$EMimBF_4$	Alg/ACFC	88 F g^{-1} @ 10 mA cm^{-2}	[49]
PAA-D-S	2 M H_2SO_4 (in situ)	PANI@CNTs	39 F g^{-1} @ 0.2 mA cm^{-2}	[47]

Additionally, the spectra suggest an ejection of the ionic aqueous solution from the hydrogel, reflected as a rise in the ionic diffusion resistance values, represented by the W on the equivalent circuit.[41] As shown in Figure 4C, the osmotic pressure removes water from the hydrogel and modifies its mechanical and electrochemical properties.[42] Therefore, along with the increased concentration of sodium ions, compaction of free vacancies occurs inside the polymeric structure, increasing its stiffness and minimizing the diffusion pathway of the hydrogel.[14a,29] The stiffness behavior of the hydrogel displayed in Figure S4E,F (Supporting Information) changes when different electrolytic solutions are swollen, demonstrating the change in stiffness behavior of the quasi-solid material swollen with different electrolytic solutions, displaying the influence of the liquid phase over the material properties.[43] In parallel to the W element, a constant phase element associated with the low-frequency region (Q_{LF}) represents the charges reaching more internal regions of the three-dimensional PPy nanostructures. The n_{LF} increase with the mechanical stress, indicating a more homogenous contact surface between the electrode and liquid phase. This can also be observed by the rise of the values of k_2, presented in Table 2, corroborating with the indication of liquid phase enclosed to inner regions of the 3D structure of PPy after the removal of mechanical stress.[8c,44] Figure S9A (Supporting Information) presents the Bode-plot analysis of the impedance spectra and the ratio k_1/k_2, respectively.

Furthermore, the data shown in Figure S9B and Table S1 (Supporting Information) show a different behavior: pristine (H_2O) and 0.1 M HNO_3 as the liquid phase, displaying slight change on the behavior and increased values of specific C_s. Moreover, the device swollen with a smaller ionic radius electrolyte displayed higher values of specific C_s, even while submitted to a mechanical stress, as shown in Figure S9C,D (Supporting Information). As for the impedance spectra presented in Figure S9E (Supporting Information), the R_{ESR} returns to a value close to the initial upon removal of the mechanical load, as the liquid phase more easily diffuses through the hydrogel matrix not heavily affected by the osmotic pressure and salting-out effect. Consequently, the stiffness of the quasi-solid electrolyte diminishes.[31] In addition, the R_{CT} values increase as the smaller charge carriers reach the internal regions of the PPy nanostructures. Moreover, with mechanical stress, the values on the parameters do not vary as much, suggesting that diffusion is not heavily affected by the displacement of the liquid phase, maintaining the material's conductivity during the stress period.

To further explore the electrochemical performance, GCPL data were evaluated and are shown in Figure 5D. Differently from the CV analysis, the as-prepared device charge–discharge curves suggest a pseudocapacitive behavior at 0.5 A g^{-1}, with a slight distortion due to internal resistance polarization. In addition, the device displayed a specific C_s of 66 F g^{-1}, akin to other hydrogel-based electrolytes, as presented in **Table 3**. Finally, adding to suitable C_s, the device showed values of specific energy and potency of 3.0 Wh kg^{-1} and 19.9 W kg^{-1}, respectively, while holding a neutral pH, suggesting an environmentally friendly device. However, upon the addition of heavy mechanical stress, the C_s was significantly reduced to 11 F g^{-1} and distorted to a more triangular aspect, in alignment with an apparent capacitor-like behavior displayed by galvanostatic curves, indicating fast electrostatic interactions, as previously indicated by the cyclic voltammograms.[45] Such a drastic behavior change can be associated with the expulsion of the liquid phase, significantly diminishing the pathway for ionic diffusion and favoring fast ionic interactions to charges confined near the electrode surface.[36] Upon removal of the mechanical stress, the C_s fell to 7 F g^{-1}, which the precipitation of sodium sulfate crystals could explain due to the salting-out effect. The hydrogel properties are highly dependent on parameters such as the type of cross-link between polymeric chains and the composition of the phases (solid-liquid), which will dictate the diffusion and mass-transfer behavior inside the gel, allowing tuning its properties based on pH, concentration, and charge, as previously presented in this work.[43,46]

To contrast to the effect of the liquid phase, characterization was performed using an acidic solution and is presented in the supplementary information of the present work (Figure S9C–F, Supporting Information). At acidic pH and when using smaller ionic species, the device's electrochemical performance was enhanced, displaying a pseudocapacitive behavior with slight changes in C_s values when submitted to mechanical stress, although minimizing the environment friendliness of the device. These results corroborate the previously presented work and highlight tunning of the system by simply swelling with different electrolytic solutions to shape the system properties.

6. Conclusions

This study presents a flexible, low-cost, quasi-solid electrochemical system with shapeable properties tuned through a simple swelling mechanism. As electrodes, graphite threads were modified with PPy nanostructures, increasing their electrochemical

properties due to the presence of polymer without affecting its flexibility or chemical stability. For electrolytes, PVA/SA hydrogel as an electrolyte prepared by the straightforward freeze–thaw method was used, where physical cross-linking occurs between the polymeric chains, producing a homogenous and porous quasi-solid material. The influence of semicrystallinity was observed in the hydrogel in diffractograms due to the presence of PVA and SA peaks at 21° 2θ and 41° 2θ, respectively. Furthermore, Nyquist spectra indicated a porous solid phase that allows the diffusion of the liquid phase of the as-prepared material, displaying ionic conductivity of 3.6 mS cm^{-1}, superior to similar hydrogels reported in the literature. Diffusional behavior was also observed through swelling experiments in as-prepared and dry conditions of the hydrogel, stabilizing after 1 h of soaking in electrolytic solutions with different pH, tunning its electrochemical and mechanical properties. Acidic pH indicated better electrochemical performance, while neutral pH suggested better mechanical performance, highlighting the versatility of this material.

The excellent performance of both materials allowed the structuration of a quasi-solid electrochemical energy storage system, displaying capacitive behavior in voltammetric experiments, varying accordingly to the liquid electrolyte swollen into the system. GPCL experiments exhibit a specific C_s of 66 F g^{-1} at 0.5 A g^{-1}. The device is comparable to similar devices reported in the literature, with a specific energy and specific power of 19.9 W kg^{-1} and 3.0 Wh kg^{-1}, respectively. However, its performance was significantly hindered when submitted to heavy loads of mechanical flexibility, decreasing its specific C_s by 88% and distorting the voltammogram.

The results obtained in this work can help improve studies on environment-friendly electrolyte quasi-solid materials. We explored different hydrogel properties, such as swell, conductivity, and tunning properties, allowing other applications ranging from sensors to energy storage systems. In addition, new functional and environmentally friendly materials are critical in developing new devices. Therefore, we present a low-cost and versatile material combining biodegradable PVA with naturally occurring SA to pair this point of importance.

7. Experimental Section

Chemicals: PVA (Mw 146 000–186 000, 99+% hydrolyzed, Sigma–Aldrich), SA (medium viscosity ≥ 2000 cP, Sigma–Aldrich), nitric acid (HNO_3, 68%, Sigma–Aldrich), MO (85%, ACS), potassium nitrate (KNO_3, 99% A.C.S, Sigma–Aldrich), sodium sulfate (Na_2SO_4, 99% P.A, Sigma–Aldrich), and conductive carbon-graphite cloth (CarbonScout) were used as received. Py monomer (98%, Sigma–Aldrich) was redistilled before use, and all solutions were prepared using ultrapure water (Elga system).

Electrode Modification and Characterization: PPy nanotubes were synthesized using chronoamperometry, applying MO as a template framework for forming nanotubes. The solution was prepared by adding 100×10^{-3} M of Py monomer into a solution containing 5×10^{-3} M of MO and 8×10^{-3} M of KNO_3, which was then sonicated for 5 min at room temperature. Finally, 650 µL of HNO_3 solution 1 M was added to reach the pH of 2, which was reported as the most suitable media for electrode modification toward supercapacitor appliances.[6a]

Graphite wire electrodes were used for the potentiostatic polymerization at −0.8 V versus Ag/AgCl (3 M) for 5 min. The modified electrodes were then cleaned with deionized water and dried in an oven at 60 °C for 4 h. After drying, the electrodes were ready for characterization.

Before characterization experiments, the samples were washed three times with distilled water and ethanol (50% by volume) and dried in the oven at 60 °C for 4 h. After drying, TEM samples were dispersed in ethanol and dropped in a copper sample holder. For FTIR analysis, samples were dried and grounded, and mixed with KBr to prepare pellets. The mass of electrodeposition was measured through gravimetric difference using a microbalance Metter-Toledo XSE205DU.

The surface modification and deposition of PPy nanotubes on the electrodes were investigated by SEM using a TESCAN VEGA3 LMU in High Vacuum Mode with a resolution of 3 nm at 30 kV. In addition, TEM was performed with a 2100F system (JEOL) at a voltage of 200 kV. To prepare the samples, a copper grid coated with lacey carbon was used as the sample holder, and the modified graphite threads were cut and dispersed in ethanol via ultrasonic bath and then dried on the copper grid drop by drop. FTIR spectra were obtained on a Bruker Vertex 70 BRUKER using an attenuated total reflectance method.

Raman analysis was carried out using a Renishaw InVia microscope with an excitation laser of 633 nm excitation wavelength with a power of 87 µW at the focal point of the sample with a numeric aperture of 0.75. For each sample, spectra from 10 points were recorded with 20 s exposure time and accumulated five times. The samples were placed on a glass slide, and the system was calibrated with a silicon single crystal.

X-ray diffraction was carried out with a D8 Advance system (Bruker) with wide-angle analysis at room temperature, with a copper source (Cu-Kα, 40 kV, 40 mA). The 2θ range of 10–50° was scanned at a rate of 0.005 s^{-1}. The samples were mounted on a glass slide for the measurement, and the system was calibrated using a corundum standard.

The electrochemical measurements were done using an AUTOLAB PSTAT204 and Gamry Reference 3000 potentiostats, used as working electrode graphite wires (pure and modified) normalized by weight, a platinum mesh (1 cm^2) as counter-electrode and Ag/AgCl (3 M) reference electrode. To evaluate the electrochemical influence and stability of the electrode modification, the cells were initially analyzed by CV in a potential window ranging from −1.0 to +0.5 V at different scan rates (20–100 mV s^{-1}) in an aqueous electrolyte solution of 0.5 M Na_2SO_4. Next, EIS was performed from 100 kHz to 10 mHz at an open circuit potential (OCP) of 0.06 V versus Ag/AgCl, measured for 1 h before the experiment.

Hydrogel Preparation and Characterization: The PVA-based hydrogel preparation occurred by the freezing–thawing method.[12c,16] The ratio between PVA:SA used was (10:1). For preparing 20 mL of hydrogel, 1 g of PVA and 0.1 g of SA were thoroughly mixed and solubilized in 20 mL of deionized water. The dispersion was then heated to 85 °C and stirred for 3 h until reaching a glue-like dense solution. Next, the solution was cooled to room temperature and frozen for 20 h. The quasi-solid hydrogel was then thawed and allowed to reach room temperature to be frozen and thawed again. After 20 h of freezing, the hydrogel was thawed and dried at room temperature for 5 h. Then it was ready to be swollen in different electrolytic solutions and submitted for electrochemical evaluation.

The morphology was characterized using as-prepared and freeze-dried samples by SEM using a ZEISS GEMINI 500 microscope coupled with an Xmax detector from Oxford instruments employing an acceleration voltage of 0.5–5 kV for imaging. The samples were mounted on an aluminum stub fixed with copper tape with an extra conductive sputter of a 6 nm thick coating of platinum.

The hydrogel was electrochemically characterized after being swollen with solutions of distilled water, 0.5 M Na_2SO_4, and 0.1 M HNO_3, where the mass variation was measured to investigate the uptake of electrolyte solution. CV experiments allowed the investigation of chemical stability in a potential window of −0.8 to +0.8 V, using a classic three-cell electrode system with two stainless steel mesh as counter and the working electrode (with an area of 0.785 cm^2) at different scan rates (10-100 mV s^{-1}).

EIS experiments were performed in a two-electrode configuration using a Metrohm Autolab PGSTAT208 and BioLogic VMP-300 potentiostats, with frequencies ranging from 100 kHz to 100 mHz versus OCP to investigate the ionic conductivity (σ) of the hydrogel at room temperature. The EIS spectra were recorded, and the ionic conductivity was determined using

Equation (1), indicated below.[17]

$$\sigma = \frac{T}{A} \times \frac{1}{Rs} \quad (1)$$

where T is the gel thickness (1 cm), R_s is the hydrogel bulk resistance, and A is the area of the hydrogel exposed to the electrodes (0.785 cm^2).

The swelling degree (SD) of the hydrogel was investigated in samples prepared (wet) and dried (dry) in an oven for 3 h at 40°. In addition, a different set of samples were soaked for 1 h in distilled water and in solutions of KCL 10% (mass/volume; pH 7.48), 0.5 M Na_2SO_4 (pH 7.15), 0.1 M H_3PO_4 (pH 4.22) and 0.1 M HNO_3 (pH 2.37). During the soaking period, the mass of the samples was measured in intervals of 5 min, and the SD was determined using Equation (2).[18]

$$SD = \frac{W_t - W_i}{W_i} \times 100\% \quad (2)$$

where W_t is the mass of the sample at a time t, and W_i is the mass of the initial sample.

The influence of the freeze–thaw method over the interaction between the polymeric chains of PVA and SA was investigated. XRD was performed on samples dried in the oven at 40 °C for 3 h and samples swollen with distilled water. The XRD experiments were carried out at room temperature using a D8 Advance (BRUKER) with a copper source (Cu-Kα, 40 kV, 40 mA). The 2θ angle range from 10° to 60° was scanned at a rate of 0.005° s^{-1}.

Quasi-Solid-State Device Assembly: Two modified electrodes were parallelly placed in the hydrogel before the first freezing step during the hydrogel synthesis. After that, the system followed the hydrogel synthesis procedure. The raw prototype was ready upon reaching room temperature at the final thawing, followed by an evaporation period of 2 h at room temperature. Then, the prototype was inserted into a pouch bag containing 2 mL of 0.5 M Na_2SO_4 solution and sealed. Finally, the supercapacitor prototype was ready to undergo electrochemical characterization. A schematic diagram of this process is presented in Figure S7 (Supporting Information).

Supporting Information

Supporting Information is available from the Wiley Online Library or from the author.

Acknowledgements

The authors thank the Institutos LACTEC for all the support during this work's development, contributing to infrastructure and financial support. Prof. Dr. Olfa Kanoun (Mess- und Sensortechnik – Technische Universität Chemnitz) is thanked for the infrastructure and equipment to perform mechanical experiments in this work. E.P. thanks the Alexander-von-Humboldt Foundation for their support. The author thank the Brazilian funding agencies CAPES, CNPq (303038/2019-5; 408635/2018-5), and Fundacao Araucaria for financial support. We also acknowledge funding via INCT in Bioanalytics (FAPESP grant no. 2014/50867-3 and CNPq grant no. 465389/2014/2014/7).

Open access funding enabled and organized by Projekt DEAL.

Conflict of Interest

The authors declare no conflict of interest.

Author Contributions

J.G.A.R. investigated the work, performed data curation, performed visualization, and wrote the original draft. A.E.D. performed methodology, reviewed and edited the work. E.P. performed the methodology, investigation, data curation, and reviewed and edited the work. V.P. performed visualization, conceptualization, data curation, and reviewed and edited the work. M.V. performed conceptualization, data curation, visualization, project administration, and supervision and reviewed and edited the work, .

Data Availability Statement

The data that support the findings of this study are available from the corresponding author upon reasonable request.

Keywords

electrolyte, flexible energy storage, hydrogel, modified electrode

Received: May 6, 2023
Revised: June 10, 2023
Published online: July 23, 2023

[1] a) W. Zhao, L. Wei, Q. G. Fu, X. Guo, *J. Power Sources* **2019**, *422*, 73; b) C. V. V. Muralee Gopi, R. Vinodh, S. Sambasivam, I. M. Obaidat, H.-J. Kim, *J. Energy Storage* **2020**, *27*, 101035.

[2] a) S. Arepalli, H. Fireman, C. Huffman, P. Moloney, P. Nikolaev, L. Yowell, K. Kim, P. A. Kohl, C. D. Higgins, S. P. Turano, W. J. Ready, *JOM* **2005**, *57*, 26; b) F. Beguin, V. Presser, A. Balducci, E. Frackowiak, *Adv. Mater.* **2014**, *26*, 2219; c) E. E. Miller, Y. Hua, F. H. Tezel, *J. Energy Storage* **2018**, *20*, 30; d) N. Jäckel, D. Weingarth, A. Schreiber, B. Krüner, M. Zeiger, A. Tolosa, M. Aslan, V. Presser, *Electrochim. Acta* **2016**, *191*, 284; e) J. K. Ewert, D. Weingarth, C. Denner, M. Friedrich, M. Zeiger, A. Schreiber, N. Jäckel, V. Presser, R. Kempe, *J. Mater. Chem. A* **2015**, *3*, 18906.

[3] a) Z. Lin, E. Goikolea, A. Balducci, K. Naoi, P. L. Taberna, M. Salanne, G. Yushin, P. Simon, *Mater. Today* **2018**, *21*, 419; b) M. Mirzaeian, Q. Abbas, A. Ogwu, P. Hall, M. Goldin, M. Mirzaeian, H. F. Jirandehi, *Int. J. Hydrogen Energy* **2017**, *42*, 25565; c) R. N. Yogamalar, K. Sharma, P. M. Shafi, *J. Energy Storage* **2022**, *55*, 105727; d) Q. H. Zhou, H. Y. Yao, *Energy Rep.* **2022**, *8*, 656.

[4] a) D. Kasprzak, C. C. Mayorga-Martinez, M. Pumera, *Energy Fuels* **2023**, *37*, 74; b) K. Jost, C. R. Perez, J. K. McDonough, V. Presser, M. Heon, G. Dion, Y. Gogotsi, *Environ. Sci.* **2011**, *4*, 5060.

[5] a) P. Simon, Y. Gogotsi, *Philos. Trans. R. Soc., A* **2010**, *368*, 3457; b) P. Simon, Y. Gogotsi, *Nat. Mater.* **2020**, *19*, 1151; c) S. Fleischmann, J. B. Mitchell, R. Wang, C. Zhan, D. E. Jiang, V. Presser, V. Augustyn, *Chem. Rev.* **2020**, *120*, 6738; d) S. Karthikeyan, B. Narenthiran, A. Sivanantham, L. D. Bhatlu, T. Maridurai, *Mater. Today Proc.* **2021**, *46*, 3984.

[6] a) D. Kałuża, M. Gniadek, A. Michalska, K. Maksymiuk, *Electrochim. Acta* **2019**, *320*, 134585; b) Z. F. Wang, M. S. Zhu, Z. X. Pei, Q. Xue, H. F. Li, Y. Huang, C. Y. Zhi, *Maer. Sci. Eng., R* **2020**, *139*, 100520; c) N. N. Loganathan, V. Perumal, B. R. Pandian, R. Atchudan, T. N. J. I. Edison, M. Ovinis, *J. Energy Storage* **2022**, *49*, 104149; d) A. Sangili, B. Unnikrishnan, A. Nain, Y. J. Hsu, R. S. Wu, C. C. Huang, H. T. Chang, *Energy Storage Mater.* **2022**, *53*, 51; e) S. Fleischmann, Y. Zhang, X. Wang, P. T. Cummings, J. Wu, P. Simon, Y. Gogotsi, V. Presser, V. Augustyn, *Nat. Energy* **2022**, *7*, 222.

[7] a) Q. F. Meng, K. F. Cai, Y. X. Chen, L. D. Chen, *Nano Energy* **2017**, *36*, 268; b) S. Ghosh, T. Maiyalagan, R. N. Basu, *Nanoscale* **2016**, *8*, 6921.

[8] a) A. A. B. Hamra, H. N. Lim, S. M. Hafiz, S. Kamaruzaman, S. A. Rashid, R. Yunus, M. Altarawneh, Z. T. Jiang, N. M. Huang, *Electrochim. Acta* **2018**, *285*, 9; b) Q. Z. Liu, B. Wang, J. H. Chen, F. Li,

K. Liu, Y. D. Wang, M. F. Li, Z. T. Lu, W. W. Wang, D. Wang, *Composites, Part A* **2017**, *101*, 30; c) L. F. Marchesi, F. R. Simoes, L. A. Pocrifka, E. C. Pereira, *J. Phys. Chem. B* **2011**, *115*, 9570; d) A. Rudge, J. Davey, I. Raistrick, S. Gottesfeld, J. P. Ferraris, *J. Power Sources* **1994**, *47*, 89.

[9] a) Q. Y. Dou, S. L. Lei, D. W. Wang, Q. N. Zhang, D. W. Xiao, H. W. Guo, A. P. Wang, H. Yang, Y. L. Li, S. Q. Shi, X. B. Yan, *Environ. Sci.* **2018**, *11*, 3212; b) G. H. Lane, E. Jezek, *Electrochim. Acta* **2014**, *150*, 173; c) C. Zhong, Y. Deng, W. Hu, J. Qiao, L. Zhang, J. Zhang, *Chem. Soc. Rev.* **2015**, *44*, 7484.

[10] H. Schranger, F. Barzegar, Q. Abbas, *Curr. Opin. Electrochem.* **2020**, *21*, 167.

[11] P. Rahmani, A. Shojaei, *Adv. Colloid Interface Sci.* **2021**, *298*, 102553.

[12] a) R. J. Fong, A. Robertson, P. E. Mallon, R. L. Thompson, *Polymers* **2018**, *10*, 1036; b) S. Gupta, T. J. Webster, A. Sinha, *J. Mater. Sci.: Mater. Med.* **2011**, *22*, 1763; c) R. Ricciardi, F. Auriemma, C. De Rosa, F. Laupretre, *Macromolecules* **2004**, *37*, 1921; d) J. L. Holloway, K. L. Spiller, A. M. Lowman, G. R. Palmese, *Acta Biomater.* **2011**, *7*, 2477.

[13] a) Y. Li, X. Liu, Q. Gong, Z. Xia, Y. Yang, C. Chen, C. Qian, *Int. J. Biol. Macromol.* **2021**, *172*, 41; b) Y. J. Kim, J. Min, *Int. J. Biol. Macromol.* **2021**, *193*, 1068.

[14] a) B. L. Guo, A. Finne-Wistrand, A. C. Albertsson, *Chem. Mater.* **2011**, *23*, 1254; b) P. Candry, B. J. Godfrey, Z. Wang, F. Sabba, E. Dieppa, J. Fudge, O. Balogun, G. Wells, M. H. Winkler, *Sci. Rep.* **2022**, *12*, 20822.

[15] a) G. Wu, K. Jin, L. Liu, H. Zhang, *Soft Matter* **2020**, *16*, 3319; b) X. J. Gao, Q. Z. Hu, K. J. Sun, H. Peng, X. Xie, H. A. Hamouda, G. F. Ma, *J. Alloys Compd.* **2021**, *888*, 161554; c) L. Tang, S. Wu, J. Qu, L. Gong, J. Tang, *Materials* **2020**, *13*, 3947.

[16] a) M. Bahadoran, A. Shamloo, Y. D. Nokoorani, *Sci. Rep.* **2020**, *10*, 7342; b) H. Adelnia, R. Ensandoost, S. S. Moonshi, J. N. Gavgani, E. I. Vasafi, H. T. Ta, *Eur. Polym. J.* **2022**, *164*, 110974.

[17] a) S. S. Azahar, T. S. Hamidon, A. F. A. Latip, M. H. Hussin, *Chem. Phys. Impact* **2021**, *3*, 100055; b) G. Ruano, J. I. Iribarren, M. M. Perez-Madrigal, J. Torras, C. Aleman, *Polymers* **2021**, *13*, 1337.

[18] P. T. S. Kumar, G. Praveen, M. Raj, K. P. Chennazhi, R. Jayakumar, *RSC Adv.* **2014**, *4*, 65081.

[19] C. Wei, Q. Xu, Z. Chen, W. Rao, L. Fan, Y. Yuan, Z. Bai, J. Xu, *Carbohydr. Polym.* **2017**, *169*, 50.

[20] J. Ji, X. Zhang, J. Liu, L. Peng, C. Chen, Z. Huang, L. Li, X. Yu, S. Shang, *Mater. Sci. Eng., B* **2015**, *198*, 51.

[21] a) J. Zhang, Y. Liu, H. J. Guan, Y. F. Zhao, B. Zhang, *J. Alloys Compd.* **2017**, *721*, 731; b) A. E. Deller, A. L. Soares, J. Volpe, J. G. A. Ruthes, D. E. P. Souto, M. Vidotti, *Biosensors* **2022**, *12*, 970; c) B. M. Hryniewicz, J. Volpe, L. Bach-Toledo, K. C. Kurpel, A. E. Deller, A. L. Soares, J. M. Nardin, L. F. Marchesi, F. F. Simas, C. C. Oliveira, L. Huergo, D. E. P. Souto, M. Vidotti, *Mater. Today Chem.* **2022**, *24*, 100817; d) Y. Li, P. Bober, M. Trchova, J. Stejskal, *J. Mater. Chem. C* **2017**, *5*, 4236.

[22] a) M. J. L. Santos, A. G. Brolo, E. M. Girotto, *Electrochim. Acta* **2007**, *52*, 6141; b) L. Y. Li, J. Xu, M. J. Shi, J. He, J. T. Jiang, K. Dai, Z. M. Jiang, C. Yan, *Mater. Design* **2022**, *217*, 110606; c) M. Varga, D. Kopecky, J. Kopecka, I. Krivka, J. Hanus, A. Zhigunov, M. Trchova, M. Vrnata, J. Prokes, *Eur. Polym. J.* **2017**, *96*, 176; d) T. Liu, L. Finn, M. Yu, H. Wang, T. Zhai, X. Lu, Y. Tong, Y. Li, *Nano Lett.* **2014**, *14*, 2522.

[23] a) B. M. Hryniewicz, R. V. Lima, F. Wolfart, M. Vidotti, *Electrochim. Acta* **2019**, *293*, 447; b) G. Ćirić-Marjanović, S. Mentus, I. Pašti, N. Gavrilov, J. Krstić, J. Travas-Sejdic, L. T. Strover, J. Kopecká, Z. Moravková, M. Trchová, J. Stejskal, *J. Phys. Chem. C* **2014**, *118*, 14770.

[24] T. Amemiya, K. Hashimoto, A. Fujishima, *J. Phys. Chem.* **2002**, *97*, 9736.

[25] H. Fu, Z.-j. Du, W. Zou, H.-q. Li, C. Zhang, *J. Mater. Chem. A* **2013**, *1*, 14943.

[26] L. F. Marchesi, S. C. Jacumasso, R. C. Quintanilha, H. Winnischofer, M. Vidotti, *Electrochim. Acta* **2015**, *174*, 864.

[27] J. Yan, Z. Fan, T. Wei, W. Qian, M. Zhang, F. Wei, *Carbon* **2010**, *48*, 3825.

[28] J. Wu, X. Gong, Y. Fan, H. Xia, *Soft Matter* **2011**, *7*, 6205.

[29] H. S. Samanta, S. K. Ray, *Carbohydr. Polym.* **2014**, *99*, 666.

[30] a) I. Khalid, M. Ahmad, M. U. Minhas, K. Barkat, *Polym. Bull.* **2018**, *75*, 1075; b) B. Mandal, S. K. Ray, *Carbohydr. Polym.* **2013**, *98*, 257.

[31] X. Jiang, N. Xiang, H. Zhang, Y. Sun, Z. Lin, L. Hou, *Carbohydr. Polym.* **2018**, *186*, 377.

[32] M. Jiang, J. Zhu, C. Chen, Y. Lu, Y. Ge, X. Zhang, *ACS Appl. Mater. Interfaces* **2016**, *8*, 3473.

[33] C. Zhao, C. Wang, Z. Yue, K. Shu, G. G. Wallace, *ACS Appl. Mater. Interfaces* **2013**, *5*, 9008.

[34] G. Zhou, L. Yang, W. Li, C. Chen, Q. Liu, *iScience* **2020**, *23*, 101502.

[35] a) M. M. Abudabbus, I. Jevremović, K. Nešović, A. Perić-Grujić, K. Y. Rhee, V. Mišković-Stanković, *Composites, Part B* **2018**, *140*, 99; b) Y. Bu, H.-X. Xu, X. Li, W.-J. Xu, Y.-x. Yin, H.-l. Dai, X.-b. Wang, Z.-J. Huang, P.-H. Xu, *RSC Adv.* **2018**, *8*, 10806.

[36] K. Aoki, B. Wang, J. Y. Chen, T. Nishiumi, *Electrochim. Acta* **2012**, *83*, 348.

[37] A. C. F. Ribeiro, I. Fabela, A. J. F. N. Sobral, L. M. P. Verissimo, M. C. F. Barros, M. M. Rodrigo, M. A. Esteso, *J. Chem. Thermody.* **2014**, *74*, 263.

[38] Y. Bai, R. Liu, Y. Wang, H. Xiao, Y. Liu, G. Yuan, *ACS Appl. Mater. Interfaces* **2019**, *11*, 43294.

[39] Q. M. Tu, L. Q. Fan, F. Pan, J. L. Huang, Y. Gu, J. M. Lin, M. L. Huang, Y. F. Huang, J. H. Wu, *Electrochim. Acta* **2018**, *268*, 562.

[40] J. Bisquert, *Electrochim. Acta* **2002**, *47*, 2435.

[41] D. R. Franceschetti, J. R. Macdonald, R. P. Buck, *J. Electrochem. Soc.* **1991**, *138*, 1368.

[42] T. M. C. Maria, R. A. de Carvalho, P. J. A. Sobral, A. M. B. Q. Habitante, J. Solorza-Feria, *J. Food Eng.* **2008**, *87*, 191.

[43] N. Paradee, A. Sirivat, S. Niamlang, W. Prissanaroon-Ouajai, *J. Mater. Sci.: Mater. Med.* **2012**, *23*, 999.

[44] B. A. Mei, O. Munteshari, J. Lau, B. Dunn, L. Pilon, *J. Phys. Chem. C* **2018**, *122*, 194.

[45] C. Jiang, M. Gao, S. Zhang, L. Huang, S. Yu, Z. Song, Q. Wu, *Int. J. Biol. Macromol.* **2023**, *225*, 1437.

[46] C. J. Silsby, J. R. Counts, T. A. Christensen, M. F. Roll, K. V. Waynant, J. G. Moberly, *ACS ES&T Eng.* **2022**, *2*, 1896.

[47] L. Y. Yang, G. B. Zhou, Y. J. Jin, Y. Sun, Q. Liu, C. Y. Chen, *J. Power Sources* **2022**, *548*, 232015.

[48] H. H. Rana, J. H. Park, E. Ducrot, H. Park, M. Kota, T. H. Han, J. Y. Lee, J. Kim, J. H. Kim, P. Howlett, M. Forsyth, D. MacFarlane, H. S. Park, *Energy Storage Mater.* **2019**, *19*, 197.

[49] K. Soeda, M. Yamagata, M. Ishikawa, *J. Power Sources* **2015**, *280*, 565.